

Laser Frequency Combs with Fast Gain Recovery: Physics and Applications

Marco Piccardo* and Federico Capasso

The dynamics of semiconductor lasers with fast gain is generally considered to suppress amplitude modulation, resulting in a frequency-modulated output. Since their first demonstration of frequency comb operation, quantum cascade lasers—ideal representatives of this class of lasers with fast gain dynamics—were indeed shown to emit frequency-modulated combs. The understanding of these frequency comb regimes has progressively evolved, being refined from simpler arguments to more advanced theories, considering the role of Kerr nonlinearity and linewidth enhancement factor. By now, the traditional frequency-modulated combs are rather well understood in quantum cascade lasers, but new types of frequency combs have emerged, reopening interesting physics questions in these lasers. Recent advancements on two open frontiers will be discussed: harmonic frequency combs, characterized by mode skipping of many free spectral ranges, and spatiotemporal structures with solitonic features, recently reported in unidirectional ring cavities. These new types of frequency combs open technological and fundamental perspectives, sprouting new interest in quantum cascade lasers.

1. Introduction

The study of laser dynamics boomed in the 1960s when the first observations of energetic pulses—a phenomenon originally called spiking^[1]—in the emission of solid-state lasers motivated a thorough investigation of multimode behavior and self-locking. The following decades witnessed fundamental advances in the understanding of nonlinear laser dynamics^[2] going hand in hand with technological progress in the stabilization of an output train


of pulses from mode-locked lasers, resulting in strictly periodic waveforms corresponding to a comb of optical frequency modes equally spaced by extreme accuracy. Precision^[3] is the keyword that defined the development of optical frequency combs (OFCs) and consequent impact on our society: OFCs are today a pillar in the field of optics, acknowledged by one half of the Nobel Prize in Physics shared in 2005 by Theodor W. Hänsch and John L. Hall. OFCs revolutionized optical clocks, linking radiofrequency standards to optical frequencies, as well as metrology, high-precision spectroscopy, and communications.^[4–6]

Following the first tabletop sources, frequency comb generators progressively evolved, also shrinking in size, eventually making available chip-scale OFC platforms with great benefits in terms of portability. Today, there are many types of frequency combs, not only in terms of

size, but also in terms of spectral range of emission, which covers, by combining all sources, the entire electromagnetic spectrum, from the terahertz to the deep ultraviolet region. Considering that such a wide range of sources exists, an important aspect to consider in order to distinguish them is the specific laser dynamics they follow. This is dictated by a set of laser parameters and defines the temporal characteristics of the emitted waveform. A common criterion of classification in laser dynamics is the one introduced by Tito Arecchi.^[2,7] This consists in dividing lasers in three classes—class A, B and C—depending on the relative magnitude of three fundamental dynamical parameters related to material (i.e., population inversion and macroscopic polarization) and field variables: the carrier relaxation time or gain recovery time T_1 , the polarization relaxation time T_2 (corresponding to the half-width of the spectral bandwidth) and the photon lifetime T_c , proportional to the cavity Q -factor (See Table 1). Moreover, depending on the laser class, a different set of Lamb's self-consistency equations,^[8,9] which involve the electric field, polarization, and population inversion, needs to be solved to determine the laser behavior. In the case of class-A lasers, only one equation is sufficient, as the active medium follows the field without delay; thus, both the inversion and polarization can be adiabatically eliminated, while in the case of class-B and C lasers, two and three equations are needed, respectively. In the context of OFCs, another important parameter determining the frequency comb dynamics is the characteristic time of intermodal beats T_{rep} , corresponding to the inverse of

M. Piccardo
Center for Nano Science and Technology
Fondazione Istituto Italiano di Tecnologia
Milano Italy
E-mail: piccardo@g.harvard.edu

M. Piccardo, F. Capasso
Harvard John A. Paulson School of Engineering and Applied Sciences
Harvard University
Cambridge, MA USA
E-mail: capasso@seas.harvard.edu

 The ORCID identification number(s) for the author(s) of this article can be found under <https://doi.org/10.1002/lpor.202100403>

© 2021 The Authors. Laser & Photonics Reviews published by Wiley-VCH GmbH. This is an open access article under the terms of the Creative Commons Attribution License, which permits use, distribution and reproduction in any medium, provided the original work is properly cited.

DOI: 10.1002/lpor.202100403

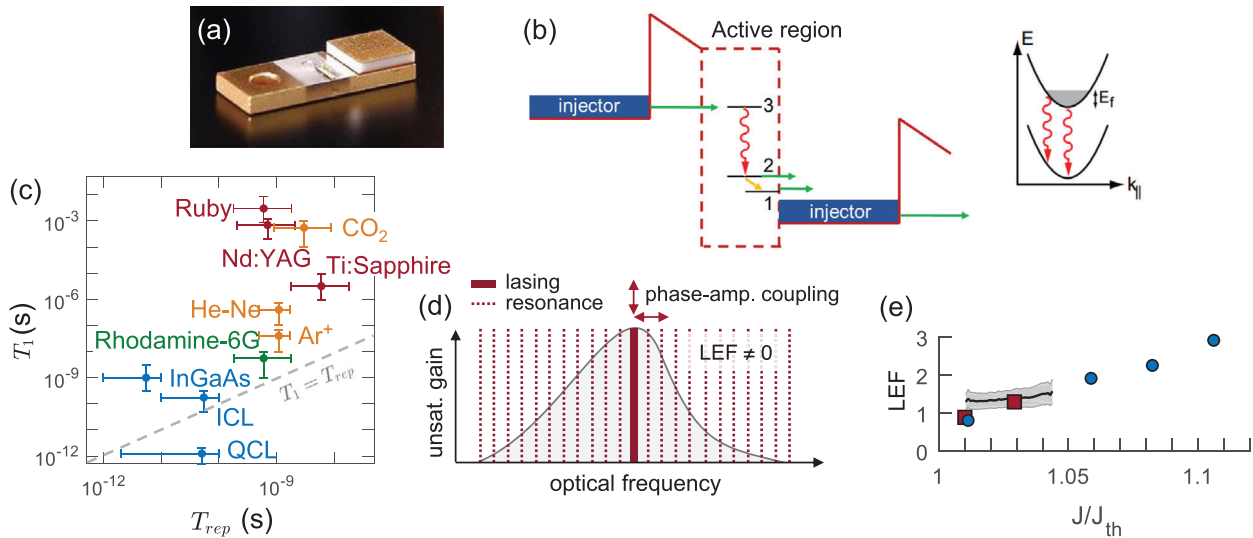


Figure 1. Dynamic laser properties resulting from intersubband transitions. a) Image of a mid-infrared Fabry–Perot QCL mounted on a chip carrier with contact pads. b) Simplified schematic of the electronic transitions involved in a QCL. Electrons enter the active region via an injector, then relax from the upper-to-lower lasing level (3 → 2) emitting a photon, and finally are extracted (2 → 1) via different mechanisms, depending on the bandstructure design. This process is repeated sequentially, as in a cascade, for each active region of the device. The gain recovery time corresponds to the time it takes for an electron to emit a photon and reach the next active region. Also shown is a schematic of the intersubband lasing transition represented in energy-momentum space. c) Characteristic timescales of the repetition period (T_{rep}) and carrier relaxation time (T_1) of solid-state (red), semiconductor (blue), gas (orange), and dye (green) lasers. Reproduced with permission.[56] Copyright 2019, American Physical Society. d) Schematic of the unsaturated gain profile of a semiconductor laser with non-zero linewidth enhancement factor (LEF) due to different factors, including the nonparabolicity of the subbands. The LEF introduces phase-amplitude coupling, connecting intensity fluctuations of the first lasing mode into a frequency shift of the cavity resonances, which can cause a multimode instability. e) Typical experimental values of the LEF measured in QCLs. Data sources: curve from ref. [26], markers from ref. [24].

Table 1. Classification of lasers depending on the characteristic laser dynamical parameters: T_1 , carrier relaxation time or gain recovery time; T_2 , macroscopic polarization relaxation time; T_c , photon lifetime.

Class-A	Class-B	Class-C
$T_1, T_2 \ll T_c$	$T_2 \ll T_c \ll T_1$	$T_c \approx T_2$

the comb spacing. The most widespread type of frequency comb generators belongs to class-B lasers, such as Ti:sapphire lasers. In this review, we will concentrate on class-A lasers and in particular on quantum cascade lasers^[10] (QCLs), a special type of semiconductor lasers (Figure 1a) characterized by an ultrashort T_1 , resulting in rich laser dynamical properties, especially in the context of OFCs.^[11]

1.1. Fast Gain Recovery

QCLs owe their fast gain dynamics to the nature of their electronic transitions. Differently from all other semiconductor lasers, QCLs rely on intersubband, rather than interband, transitions.^[12] The electronic transitions can be considered in a simplified picture as a sequential multi-step process (Figure 1b): first, electrons relax between intersubband levels in the active region; then the lower lasing level is depopulated, such as by phonon extraction combined with resonant tunneling, followed by electron transfer to the next active region. These steps repeat themselves in a cascade process that recycles the carriers for mul-

tiples photon emission through the device. The T_1 of QCLs is not simply given by the upper-to-lower level relaxation time, but it corresponds to the time it takes a carrier to relax in the active region and transport to the next active stage of the device.^[13] Typical values of T_1 for QCLs are around 1 ps for mid-infrared lasers^[14] and 5–10 ps for THz lasers^[15]—over two orders of magnitude smaller than those of interband semiconductor lasers (Figure 1c). Moreover, the T_2 of QCLs is on a sub-picosecond time scale. Therefore, by taking the example of a typical 5 mm-long Fabry–Perot cavity with facets reflectivity $R = 0.28$ and low waveguide losses (power loss coefficient, $\alpha = 1 \text{ cm}^{-1}$), we see that T_c ^[16] is around 100 ps, much larger than T_1 and T_2 , making QCLs ideal representatives of class-A lasers. Differently from the case of modelocked lasers, for which the relation $T_1 \gg T_c$ enables pulse generation using a fast saturable absorber, the opposite relation between the characteristic times of QCLs, that is $T_1 \ll T_c$, endows them with a fast saturable gain, or “reverse saturable absorber”,^[17] favoring continuous-wave emission. However, as we shall see, this intuition on the temporal behavior of QCLs turns out to be correct only to a certain extent, as pulses may also form in QCLs under some conditions, depending on the effective T_{rep} and cavity geometry.

1.2. Linewidth Enhancement Factor

There is an important point to be made about the intersubband nature of electronic transitions in QCLs. In the case of two parabolic subbands (Figure 1b), the joint density of

states is delta-like giving a gain profile very similar to those of atomic transitions. In such a system, the linewidth is expected to be symmetric and narrow, with a broadening given by the Schawlow–Townes value $\Delta\nu_{ST}$,^[18] which is connected with fluctuations due to spontaneous emission. However, the linewidth of semiconductor lasers exhibits a broadening beyond the Schawlow–Townes limit, as quantified by the linewidth enhancement factor (LEF), or α -parameter, by the relation $\Delta\nu = (1 + \alpha^2)\Delta\nu_{ST}$.^[19] The LEF couples amplitude and phase fluctuations of a lasing mode and was defined by Henry as $\alpha = (\partial n'/\partial N)/(\partial n''/\partial N)$, where n' and n'' are the real and imaginary parts of the refractive index, respectively, and N is the carrier density. In a homogeneously broadened medium lasing at the peak of the gain spectrum, the LEF is expected to be zero since $\partial n'/\partial N = 0$. However, due to the asymmetric gain profile (Figure 1d) and its effects on the refractive index dispersion via the Kramers–Kronig relations, the LEF of QCLs is non-zero. This asymmetry originates from various factors, including the non-parabolicity of the subbands, counter rotating terms,^[20] and Bloch gain,^[21] leading to an LEF of QCLs with above-threshold values measured at room temperature in the range 0.2 to 3^[22–27] (Figure 1e). This holds important consequences on OFC generation in QCLs. Fluctuations in amplitude of the first lasing mode affect, due to phase-amplitude coupling associated with the non-zero α -parameter, the position of the cavity resonances with respect to the gain peak. This allows side modes to extract more gain and start lasing, producing a multimode instability with major implications in the formation of frequency-modulated combs in Fabry–Perot QCLs,^[28] phase turbulence in free-running ring QCLs,^[26] and temporal solitons in driven ring QCLs.^[16]

1.3. From Multimode Spectra to Frequency Combs

OFCs are only a relatively recent development of QCLs. When first demonstrated in 1994, mid-infrared QCLs were multimode, low-power lasers operating in pulsed mode at cryogenic temperatures.^[10] Technological advances over the next decade allowed for an evolution toward high-power continuous-wave mid-infrared QCLs operating at room temperature. More recently, an important milestone has also been reached in THz QCLs, which have overcome the need for bulky cryogenics by being able to operate with thermoelectric coolers and becoming portable systems useful outside the laboratory.^[29] However, for a long time the multimode aspect of QCLs was seen as the effect of an incoherent instability due to an inhomogeneous distribution of carriers along the cavity—spatial hole burning—leaving little interest in these laser states.

It is only around 2007 that the hypothesis of coherent instabilities in QCLs was advanced to explain certain aspects of multimodal emission.^[30,31] A particularly interesting effect concerns the spectral evolution as a function of current, which shows in some lasers the splitting of the spectrum into two shoulders, whose separation depends on the current (Figure 2a). This was explained as Rabi splitting, induced by the Risken–Nummedal–Graham–Haken (RNGH) instability.^[32,33] The low threshold level of the multimode instability, which according to the RNGH model should occur only at a very high pumping level (about nine times the lasing threshold), was justified by showing that the in-

clusion of a saturable absorber in the Maxwell Bloch equations for the laser greatly reduces the RNGH threshold. A Kerr lensing mechanism was proposed as the origin of saturable absorption. Although the picture was not complete at the time, these early studies have been essential in indicating the possibility of frequency coherence in multimode QCL states.

The first indications of phase-locking in a QCL came in 2009 with the observation of a transition from multistability to a single stable state. The locking in this case was between transverse modes of the laser,^[34,35] existing because of the large width of the optical waveguide (Figure 2b). Locking was explained as a nonlinear coupling mechanism due to four-wave-mixing (FWM), originating from the strong optical nonlinearity of the laser transition. Coherence between longitudinal—rather than transverse—modes of the laser was shown in 2012 demonstrating a mid-infrared QCL frequency comb^[36] (Figure 2e). The constant phase relation among the emitted modes of the frequency comb is the main difference with respect to a multimode laser state. Key developments for the achievement of this milestone were the engineering of multistack active regions and the introduction of a QCL comb characterization technique called intermode beat spectroscopy (IBS). IBS measures the autocorrelation of the intermode beat, by detecting the beatnote power at the output of a Michelson interferometer gaining useful insights in the properties of the OFC. Indeed, although the measurement of a narrow intermode beatnote is a signature of frequency locking, this in itself does not give much information about the phase relationship between the modes of the frequency comb. In IBS, on the other hand, the measured beatnote interferogram provides information about the frequency versus amplitude modulation character of the emitted waveform, based on the observed dip or peak of the interferogram recorded around zero delay (Figure 2e). Following the first works in the mid-infrared, THz QCL frequency combs were demonstrated with homogeneous^[37] and heterogeneous^[38,39] designs, opening the door to precision spectroscopy, imaging, and metrology also in the terahertz range.^[40] Further efforts on dispersion engineering based on waveguide and coating designs (Figure 2c,d) optimized to reduce the net group velocity dispersion (GVD) of the laser,^[41,42] as well as more elaborate schemes based on intersubband cavity polaritons in the case of THz QCLs,^[43] allowed broadening the spectral extent of QCL combs and their current operation range.

One of the most promising applications in this field is dual-comb spectroscopy,^[44–46] in which two sources of frequency combs with a slightly different mode spacing are used to interrogate a sample and reconstruct its molecular fingerprint directly in the radiofrequency range, by detecting the optical beat between the two lasers on a fast photodetector. Starting from the first demonstration of a mid-infrared QCL dual-comb spectrometer with frequency stabilized sources^[47] followed by more recent works in the THz,^[48–50] this research has allowed the realization of spectrometers over 1000 times faster and 1000 times brighter than traditional Fourier-transform infrared spectrometers (FTIR), all without moving parts, as only a radiofrequency scan—rather than a mechanical one—is needed to reconstruct the spectrum.^[51] A priori it is not strictly necessary to have stabilized sources to obtain dual-comb measurements. In fact, it has been demonstrated that even QCL combs in free-running

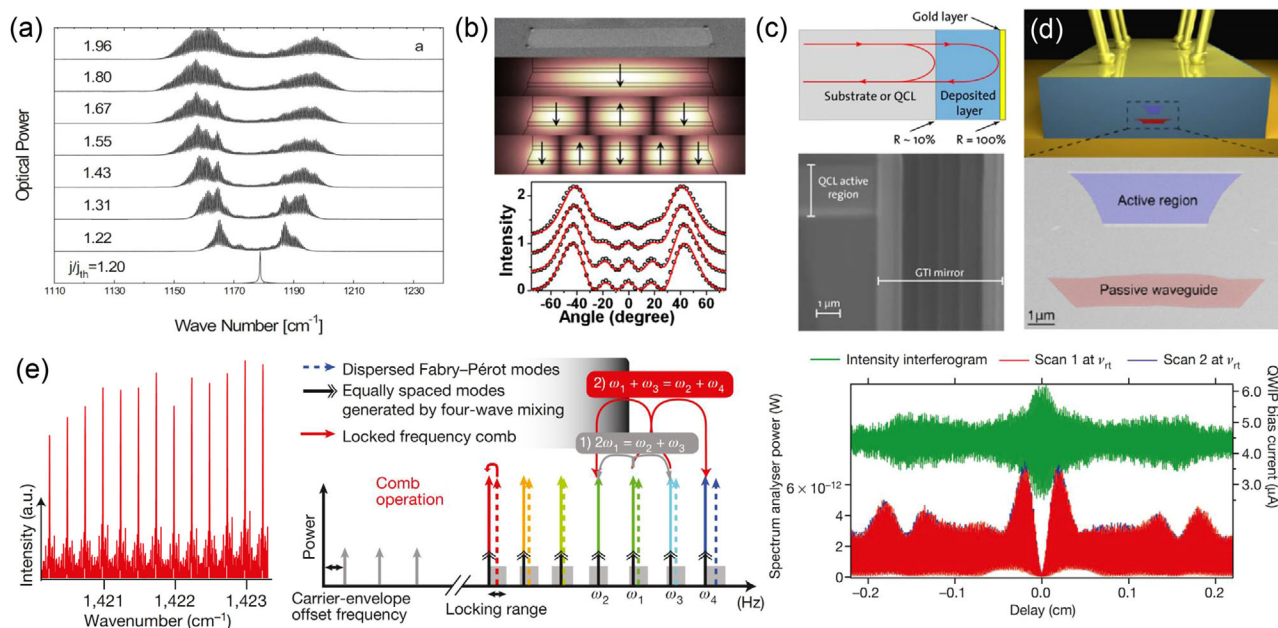


Figure 2. From multimode emission to optical frequency combs. a) Multimode optical spectra for different pumping ratios of a mid-infrared QCL exhibiting spectral splitting corresponding to twice the Rabi frequency. Reproduced with permission.^[30] Copyright 2007, American Physical Society. b) SEM image of the facet of a QCL with a 12 μm-wide active region shown with the calculated profiles of different transverse modes and polarization marked by the arrows. Coupling of the transverse modes makes a family of frequency combs, each belonging to a different transverse mode. The coherent superposition of spatial modes can be observed in the measured far-field intensity distributions. Reproduced with permission.^[34] Copyright 2009, American Physical Society. c) Schematic and SEM image of a QCL with a Gires-Tournois interferometer mirror integrated in the device as a coating to engineer the dispersion. Reproduced with permission.^[41] Copyright 2016, Optical Society of America. d) Dispersion compensation in a QCL via coupled waveguides. Reproduced with permission.^[42] Copyright 2018, Wiley-VCH. e) Magnified view of the teeth of a mid-infrared QCL frequency comb measured using a high-resolution Fourier transform infrared spectrometer, shown together with a schematic illustrating the comb formation based on four-wave mixing. Also shown are the intensity (green) and intermode beat (red) interferograms of the frequency comb. The latter allows to identify the frequency-modulated character of the emission due to the dip at delay zero. Reproduced with permission.^[36] Copyright 2012, Springer Nature.

mode are sufficient for this purpose, if the laser fluctuations are corrected by computational coherent averaging.^[52] It is to be expected, however, that the ultimate laser performance will be superior with stabilized OFC sources.^[53]

2. Physics of Frequency-Modulated Combs

The temporal nature of a comb is dictated not only by its spectral shape, but also by its phases. In fact, given a spectrum, a variation of the phases can radically alter the type of temporal waveform: from a nearly flat intensity profile to short pulses—these are the extremes (Figure 3a). Generally, OFCs can be divided into two classes, amplitude-modulated (AM)^[54] and frequency-modulated (FM)^[55,56] combs, although obviously the realm of OFCs is not dichotomous and a whole range of intermediate cases exists.^[57] One of the advantages of FM combs is their constant intensity: The fact that the power is equally distributed in time avoids waveform distortions in case of propagation in media with a nonlinear power-dependent response, like the Kerr effect. On the other hand, AM combs can exploit pulses as an additional degree of freedom to obtain temporal resolution in spectroscopic measurements, such as in pump-probe spectroscopy.

Since their first demonstration, QCL combs were thought to be primarily FM. For example in ref., [36] the IBS measurement showed a characteristic dip at zero-delay of the autocorrelation waveform which is typical of FM combs (Figure 2e). Further-

more, it was noticed that by adding a polyethylene sheet acting as an optical discriminator in front of a QCL comb, its emission was converted from FM to AM. In fact, it took many studies to fully understand the physics of FM combs in QCLs. This difficulty can be attributed to several reasons. First, the concept of fast gain recovery time is relative, since it depends on the ratio of T_1 to T_{rep} . In the case of QCL combs, depending on the beatnote frequency and therefore on the comb spacing, this can give rise to different types of temporal waveforms, more or less AM, illustrating the complex dynamics of these lasers.^[56] The degree of AM can be quantified by defining the intensity modulation depth parameter $\sigma_1 / \langle I \rangle$, where σ_1 is the standard deviation of the time-domain intensity and $\langle I \rangle$ its time-averaged value over T_{rep} .^[56,58] Another reason is related to the difficulty in measuring the phases of QCLs. IBS was a first technique that gave only a qualitative idea of the type of temporal waveform. A breakthrough came with the introduction of shifted-wave interference Fourier transform spectroscopy (SWIFTS).^[59] Similarly to IBS, SWIFTS measures the intermode beatnote interferogram using a Michelson interferometer that acts as a frequency discriminator. However, in the case of SWIFTS, not only the power of the beatnote but its two quadratures are recorded with a lock-in amplifier (Figure 3b) giving access to both the phase and amplitude distributions of the frequency comb, as well as to its temporal waveform. The reference of the lock-in amplifier is given by the laser beatnote, which is measured using a photodetector before

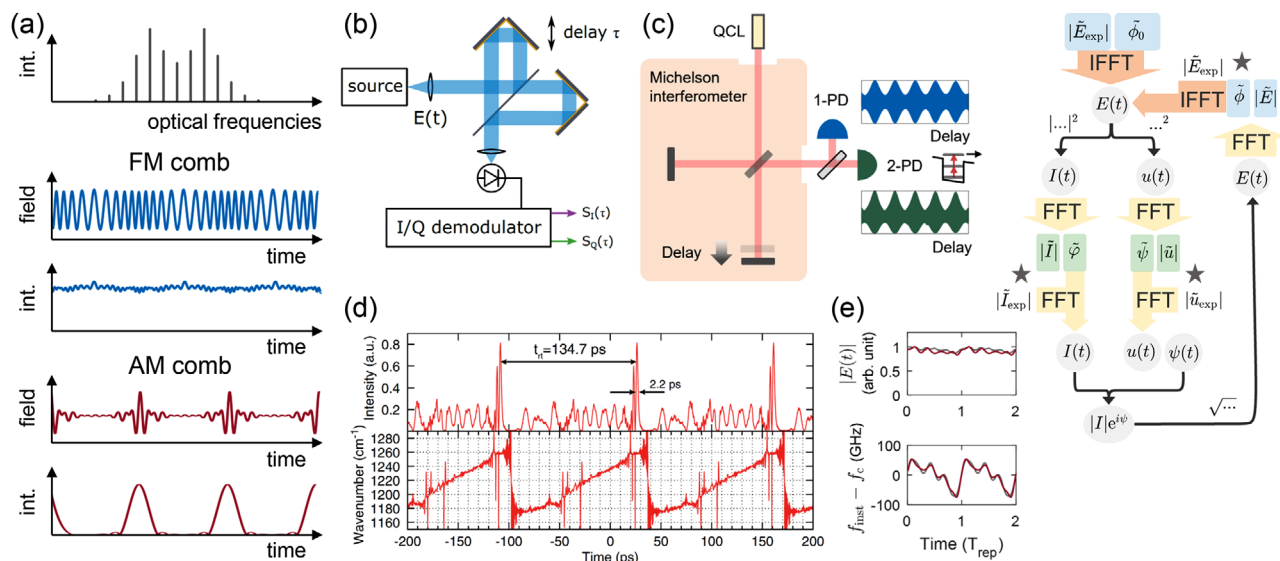


Figure 3. Characterization of frequency-modulated combs. a) Example of a frequency comb spectrum that, depending on the phase relationship among its modes, can correspond to a frequency-modulated (FM) or amplitude-modulated (AM) output. For each type of output, both the field and intensity are calculated as a function of time. In the FM comb, the intensity is nearly constant, while the frequency is modulated as a function of time, corresponding to a frequency chirp. b) Schematic of a shifted-wave interference Fourier transform spectroscopy (SWIFTS) set-up. The laser emission is spectrally analyzed using a Michelson interferometer and its output is acquired by a fast photodetector. Then, using an I/Q demodulator the two quadratures of the beatnote are retrieved, giving access to the temporal waveform of the frequency comb. Reproduced with permission.^[59] Copyright 2015, Optical Society of America. c) Schematic of a nonlinear technique for frequency comb characterization, where the optical power at the interferometer output is acquired using a linear (1-PD) and a quadratic (2-PD) photodetector. The diagram shows the scheme of the iterative phase retrieval algorithm used to reconstruct the temporal waveform from the experimental interferograms. Reproduced with permission.^[56] Copyright 2019, American Physical Society. d) Intensity and frequency chirp of a mid-infrared QCL comb characterized with SWIFTS. Reproduced with permission.^[60] Copyright 2018, Optical Society of America. e) Intensity and frequency chirp of a harmonic QCL comb spaced by eight free-spectral ranges measured with nonlinear optical detection. Reproduced with permission.^[56] Copyright 2019, American Physical Society.

the interferometer or directly extracted electrically off the chip. SWIFTS characterization of Fabry–Perot QCL combs typically shows a characteristic linear frequency chirp for fundamental combs^[60] (Figure 3d). Subsequently, nonlinear autocorrelation based on two-photon detectors (Figure 3c) confirmed this result for harmonic combs^[56] (Figure 3e). An additional technique that can be used to characterize QCL frequency combs is dual-comb multiheterodyne, where the Fourier phases of a generic OFC are extracted by direct comparison with a metrological-grade or well-characterized OFC.^[61,62] This method, called Fourier-transform analysis of comb emission (FACE), has an advantage with respect to SWIFTS that it can also be applied when the intermode beat of the frequency comb under study is not easily accessible due to photodetector bandwidth limitations, as in the case of widely spaced harmonic frequency combs. Another convenient aspect of FACE is its simultaneous and real-time characterization of several comb teeth, which is opposite to the asynchronous nature of SWIFTS that only measures relative phases of mode pairs. On the other hand, SWIFTS is more suitable to verify the existence of partial coherence, as in the case of combs affected by transients with high phase noise.^[92] Finally, the last hurdle in understanding QCL combs lied in identifying the key ingredients that account for the temporal dynamics of QCLs in the theoretical models, which have only gradually been clarified. It started with early theories of self-frequency modulation^[17] and pseudo-random comb dynamics,^[63] which correctly predicted a nearly constant power and stable comb emission but also frequency-

modulation features that were not confirmed by the subsequent experimental measurements. In THz QCLs, initial modeling studies combining four-wave-mixing, spatial hole burning, tunneling, and dispersion could reproduce rather well the experimental spectra and some characteristic time-domain features, such as a temporal switching corresponding to low and high frequency components of the spectrum.^[64] The maximum emission principle, according to which a laser with a short T_1 should minimize amplitude fluctuations and thus operate in an FM state, was then re-examined.^[56] It was found that QCLs are among the best lasers to demonstrate this principle but only as long as the reciprocal of the beatnote frequency, that is, T_{rep} , is much larger than T_1 . When $T_{\text{rep}} \approx T_1$, the maximum emission principle is not satisfied anymore, and the partial AM nature of the laser emerges. The last years have seen the most rapid development in terms of theory. Key ingredients underlying the formation of FM combs were identified, corresponding to the GVD and the already mentioned LEF, which originates from gain asymmetry and Bloch gain^[21] leading to a giant Kerr nonlinearity. LEF and GVD give are responsible for the chirped output. In addition to this, SHB triggers multimode operation, and gain saturation suppresses amplitude modulation. A master equation combining all these elements was shown to reproduce in numerical simulations all the experimental features of QCL combs, including its linear frequency chirp.^[28] Recently, the analysis of the spatiotemporal structures of FM combs allowed to deepen the origin of the QCL comb states. These were called “extendons”,

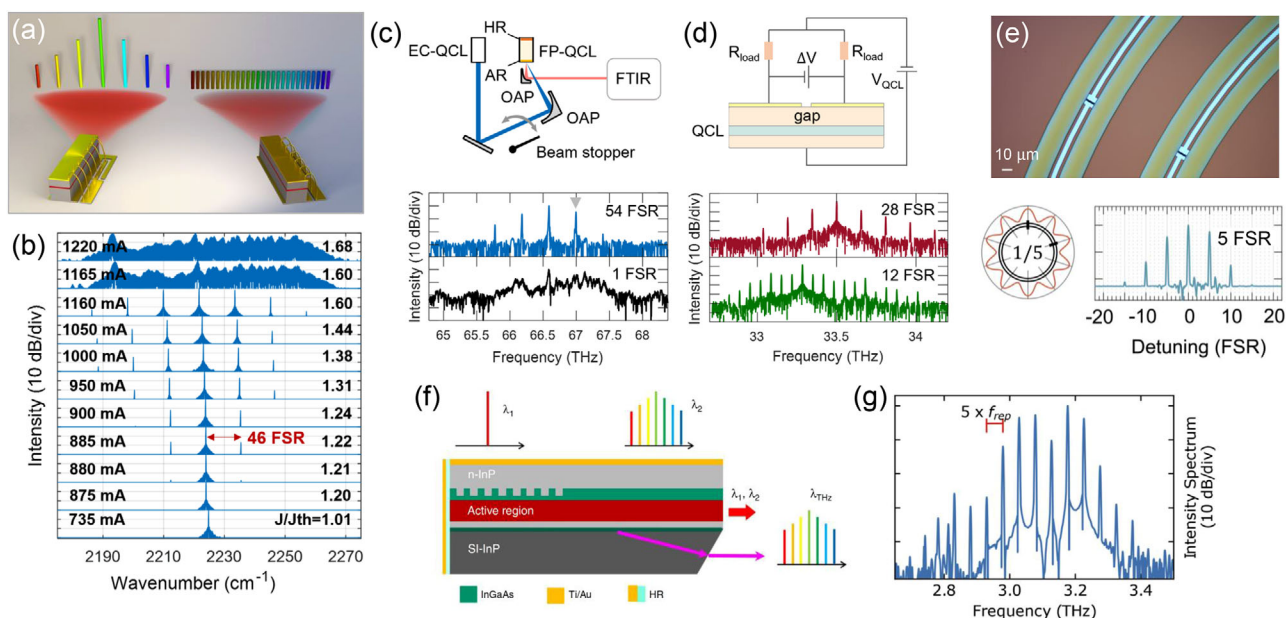


Figure 4. Generation and control of harmonic frequency combs. a) Representation of two Fabry–Perot (FP) QCLs generating a harmonic frequency comb with widely spaced modes (left) and a fundamental frequency comb spaced by 1 free-spectral range (FSR, right). b) Spectral evolution of a mid-infrared QCL as the pumping level is incremented, showing the transition from a single mode to a harmonic state spaced by 46 FSR, and finally to a fundamental frequency comb. Reproduced with permission.^[13] Copyright 2016, American Physical Society. c) Control of the spacing of a harmonic state in a FP QCL by injection of an optical seed generated from an external-cavity (EC) QCL. The frequency of the seed is marked by an arrow in the harmonic state spectrum. Adapted with permission.^[74] Copyright 2020, AIP Publishing. d) Tuning the number of skipped modes by applying a differential voltage (ΔV) in a two-section FP QCL. Reproduced with permission.^[75] Copyright 2018, Optical Society of America. e) Optical microscope image of a ring QCL with defects fabricated by optical lithography. Geometric positioning of the defects in the ring cavity allows to set the spacing of the harmonic comb. Reproduced with permission.^[77] Copyright 2021, Optical Society of America. f) Downconversion of a mid-infrared harmonic comb to the terahertz (THz) region at room temperature based on difference-frequency generation. Reproduced under terms of the CC-BY license.^[79] Copyright 2019, the Authors, published by Springer Nature. g) Self-starting harmonic frequency comb measured from a THz QCL. Reproduced with permission.^[80] Copyright 2021, AIP Publishing.

as a reference to their extended (rather than localized) occupation of the Fabry–Perot cavity, and were obtained by formulating a theoretical model inspired by the Lugiato–Lefever equation (LLE), adapted to Fabry–Perot cavities,^[65] showing that the chirp bandwidth is proportional to a combination of T_1 and T_2 . Moreover, FM combs were also shown to occur in systems with slower gain recovery times,^[55] such as quantum well and quantum dot lasers.

In the last few years, new laser states have emerged in QCLs that go beyond the FM combs discussed so far, opening new fundamental and technological perspectives in these lasers, to which we will devote the following sections.

3. Harmonic Frequency Combs

Beginning in 2014, some preliminary observations^[66–69] pointed to the ability of mid-IR and THz QCLs to skip modes and generate multimode spectra with a separation larger than one free spectral range (FSR, **Figure 4a**). These early indications culminated in the pioneering work of 2016, which revealed the entire phenomenology of the harmonic state through a systematic study of many devices with different bandstructure and emission wavelength, accompanied by a perturbative theory providing the first elements that could explain how the laser oscillates on widely spaced modes.^[13] In this work, the observation of a clear single-

mode instability threshold in continuous-wave Fabry–Perot QCLs was reported. It manifests itself in the appearance of sidebands separated by tens of FSRs from the first lasing mode, at a pump current slightly above the lasing threshold. The number of sidebands increased with increasing current while maintaining the same separation, which suggests harmonic modelocking. The low instability threshold and the large sideband spacing arise from the combination of an unclamped, incoherent Lorentzian gain due to the population grating, and a coherent parametric gain caused by temporal population pulsations that changes the spectral gain line shape. The parametric term suppresses the gain of sidebands whose separation is much smaller than the reciprocal gain recovery time, while enhancing the gain of more distant sidebands. Thus, the harmonic state is the result of the QCL acting as a self-pumped parametric oscillator.^[13] The large gain recovery frequency of the QCL compared to the FSR is essential to observe this parametric effect, which is responsible for the multiple-FSR sideband separation. This work pointed to a deep connection between parametric oscillation in optically pumped Kerr microresonators and the single-mode instability of lasers—an analogy that will be later corroborated in ring QCLs.^[16,26,62,70] In fact, one of the most intriguing features of this state is its spectral distribution, which features an intense central peak with a family of nearly symmetrical sidebands, which become progressively weaker the further they lie from the center of the

spectrum (Figure 4b). Beside this spectral indication of a parametric process underlying the formation of the harmonic state, a rigorous demonstration of its frequency comb nature was obtained by multiheterodyne measurements,^[71] based on the beating between two QCLs—one operating in the harmonic state and the other in a fundamental frequency comb state with a spacing of 1 FSR. This allowed downconverting the optical spectrum of the harmonic state into the radiofrequency regime, where the assessment of the equidistance is facilitated by established frequency counting techniques. This experiment proved that a constant phase relationship exists among the modes of the harmonic state, demonstrating that it is a frequency comb.

The harmonic state can spontaneously occur in a QCL as the injected current is increased from below threshold, provided that its GVD is low enough to be compensated by frequency pulling.^[71,72] Nevertheless, this state is fragile and is not observed in every device. This is because of its competition with multimode states spaced by 1 FSR, which can be favored, for example, when optical feedback is present in the laser.^[73] The spacing of a harmonic state spontaneously generated in a QCL can vary from a few FSRs to many tens of FSRs, depending on the device, and is very difficult to predict and engineer on the pure basis of the bandstructure. The need to generate harmonic states in a robust and deterministic way has driven researchers to explore different engineering approaches to control these states, based on optical, electrical, and radiofrequency techniques.

The optical method consists of injecting an optical seed generated with a broadly tunable laser into the QCL (Figure 4c). First, the QCL is driven at high current, where a 1 FSR-spaced fundamental state is produced. Then, injecting the optical seed into the QCL destabilizes its multimodal state—an effect due to modal competition. By adjusting the power of the optical seed, a variety of laser states can be produced within the cavity, including the harmonic state. In a specific demonstration, it was shown that the spacing could be tuned between 0.34 and 1.32 THz in a single device.^[74] A second approach is based on a multi-section Fabry–Perot device that has a gap in the top electrode and a single optical cavity^[75] (Figure 4d). By varying the current injected into the two sections of the device, it is possible to adjust their effective optical length by temperature tuning. Thus, by finely tuning the differential current, harmonic states with different spacing can be generated by this technique, albeit without deterministic control. The last method is based on the discovery that the modes of a QCL comb produce time-dependent population inversion gratings.^[76] These gratings correspond to a characteristic spatiotemporal modulation of the radiofrequency current that is determined by the comb spacing and its higher harmonics, as described by a simple analytical model. The patterns defined by the time-dependent gratings have provided a new way for the extraction and injection of RF signals into QCLs and suggested a new method to control the OFC spacing. In fact, it has been shown that by judiciously placing defects in the cavity, harmonic frequency combs with on-demand spacing can be generated, as this allows suppressing unwanted time-dependent gratings in the cavity and consequently adjusting the mode separation^[77] (Figure 4e). This is to date the most practical and robust method for generating arbitrary harmonic frequency combs, and has the advantage of being integrated, as opposed to the optical injection method that requires a separate external-cavity laser source. In

practical terms, a simple but effective way to precisely position a defect and control its reflectivity is to etch a narrow slit in the waveguide using optical lithography. It has been shown that it is necessary to introduce at least two defects into the waveguide to generate a harmonic comb, the spacing of which is dictated by the angular sector formed by the defects. This method can be seen as an analogy of colliding-pulse mode-locking for nonpulsed lasers.^[78]

The study of harmonic states is still under development. Recently, it has been shown that a mid-IR harmonic comb can be downconverted to a THz harmonic comb (Figure 4f), thus bridging these two distinct spectral regions.^[79] It has also been reported that harmonic combs can be robustly generated directly at THz frequencies using copper-based THz double-metal QCLs^[80] (Figure 4g). On the theoretical side, there is still an ongoing debate on how the harmonic state can be self-starting. The most recent advances based on time- and frequency-domain theory show that the harmonic state can be stable and self-supported under continuous pumping, but the exact conditions that trigger it are still under investigation.^[72]

The discovery of time-dependent gratings in QCLs has opened a new technological perspective for the harmonic state: using the mid-IR QCL as a photonic sub-THz generator. In fact, it must be noted that the frequencies that characterize the spacing of these combs, which can reach many hundreds of gigahertz, also correspond to oscillations of the laser population inversion. In front of this perspective, the first problem faced was to extract the radiation originating from the beating of the comb modes. To this end, the first proof of principle focused on the extraction of RF waves from a QCL operating in the fundamental comb state, spaced by 1 FSR and corresponding to 5.5 GHz.^[81] The spatial distribution of these dynamic gratings, which in the case of a fundamental comb consists of two antiphase oscillating lobes, is reminiscent of the alternating potential that exists in a dipole antenna. However, due to the metallic continuity of the electrode, most of the radiofrequency energy generated remains trapped in the laser rather than being emitted as from an antenna. The strategy put into practice was therefore to redesign the geometry of the Fabry–Perot QCL by inserting a gap to transform its contact and feed an integrated microwave antenna. This allowed emitting in free space the radiofrequencies generated by the laser, whose emission profile was characterized in an anechoic chamber. In addition to this, it was possible to encode useful information in the emitted radio signal: modulating the current of the QCL with the voltage generated at the output of an audio player, the spacing of the optical comb was modulated and therefore also the microwave signal emitted by the laser. This made it possible to wirelessly transfer a song using the QCL as a Wi-Fi radio transmitter, where the generation, modulation, and emission functions are integrated in the same device, named a laser radio transmitter.^[81] Beside current modulation, other encoding schemes are possible, such as those based on temperature tuning and the injection of radiofrequency signals, as well as using a light-emitting diode as an actuator to control comb emission.^[82]

Regarding higher-frequency generation, research has more recently begun to move in the direction of sub-THz emission by demonstrating emission from 25 to 500 GHz,^[83] albeit using the intermode beats of a THz QCL comb, rather than a mid-IR one. The laser radio transmitter concept is more general and could

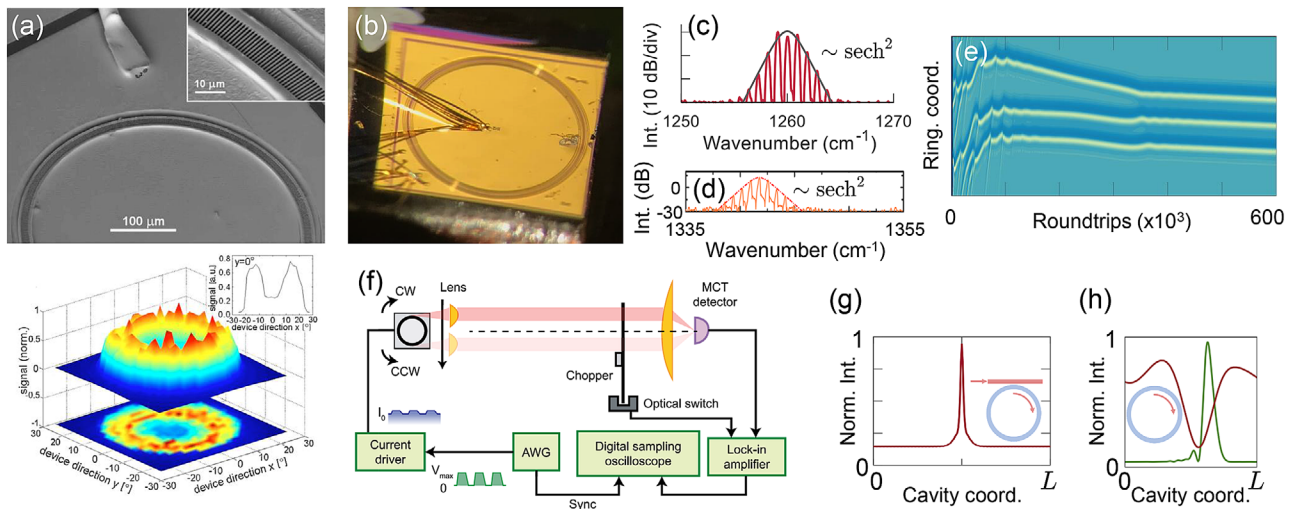


Figure 5. Laser emission enabled by the ring geometry. a) SEM image of a surface-emitting ring QCL with grating coupler shown together with the laser far-field distribution. Reproduced with permission.^[89] Copyright 2008, AIP Publishing. b) Image of an ideal ring QCL without any outcoupling structure that could perturb its intrinsic physics. c,d) Frequency combs generated by ideal rings like the one shown in (b). Top: Adapted with permission.^[26] Copyright 2020, Springer Nature; Bottom: Adapted with permission.^[90] Copyright 2020, Optical Society of America. e) Space-time diagram showing the evolution of the intensity in the ring QCL. A multimode instability is produced due to phase turbulence that, after a locking process, leads to a stable pattern, corresponding to a frequency comb. Reproduced with permission.^[26] Copyright 2020, Springer Nature. f) Experimental set-up used to identify the clockwise (CW) or counter-clockwise (CCW) operation of the ring laser. g) Temporal soliton profile predicted by theory in an externally driven ring QCL. Reproduced with permission.^[16] Copyright 2021, American Physical Society. h) Measured dissipative Kerr soliton (green curve) coexisting with a dispersive wave (red curve) from a free-running ring QCL. Data source: ref. [62].

also be implemented using for example quantum dots, which have recently been shown to behave as fast gain media.^[84] In this platform, the concept of RF generation in a laser was already proposed in 2009,^[85] but using saturable absorbers and without exploiting laser gratings nor modulating the carrier to encode information. By combining the methods of harmonic state control, sub-THz radiation extraction, and high-frequency modulation for information encoding, research on the laser radio could have an impact in the future of ultrafast sub-terahertz wireless communications,^[86–88] once the device is properly optimized for better RF coupling^[81] (e.g., by adding a thick dielectric spacer between the top and ground QCL contacts). One of the advantages of harmonic combs over fundamental combs for this type of application is that the higher frequency tones generated by the beating of the few powerful modes of the harmonic state is stronger (by approximately 37 dB, based on the analysis of ref. [81]), especially since we know that the higher the intermode separation, the more difficult it is for the laser to suppress intensity modulation. In terms of sub-THz energy extraction, it was realized that the best geometry for a laser radio is not the Fabry–Perot geometry, since in this case also mid-infrared light is emitted from the laser without any use, but rather the ring geometry, in which light is kept inside the resonator and the threshold current density is several times lower. The efforts to demonstrate ring QCL combs opened a whole new chapter in QCL research that we will discuss in the next section.

4. Ring Frequency Combs

The ring geometry has been utilized in QCLs since more than a decade.^[89] However, the goal of the first investigations was to

fabricate surface-emitting lasers to benefit from integrability into 2D arrays and on-wafer testing. To this end, these early devices featured lithographically written gratings around the perimeter of the ring to allow extraction of the optical beam in the far field (Figure 5a). Although interesting from a technological point of view, these lasers did not allow the study of the intrinsic physics of a QCL ring, due to the perturbation caused by the surface gratings. It is only very recently that interest in the exploration of QCL rings with an ideal cavity (Figure 5b) started to arise.^[26,90] In principle, from this type of cavity, one would expect single mode emission throughout the laser operating range, unlike Fabry–Perot cavities. In fact, it is a common notion that in a ring laser where there are no counter-propagating waves—because of the absence of an intra-cavity reflection element—a multimode state cannot be generated, except at an extremely high, and often unachievable, laser pumping level of nine times the lasing threshold.^[32,33] However, with much surprise, two recent studies have found that QCL rings exhibit a multimode transition at low injection current and generate frequency combs, albeit with different spectral characteristics than Fabry–Perot lasers. In particular, the spectra emitted by QCL rings consist of a set of grouped modes with a characteristic sech^2 -type envelope (Figure 5c,d). For the purpose of control, QCL rings integrating a small defect in the waveguide were also fabricated to induce counter-propagating waves,^[26] showing a different spectral emission similar to that of Fabry–Perot QCLs, which is dominated by SHB.

The observation of combs in defect-free QCL rings challenged established notions in the field. This has led to the discovery that the initial single-mode state of the laser is destabilized due to a phase turbulence phenomenon^[26] (Figure 5e) described by Ginzburg–Landau theory and common to many physical

systems, such as superconductors and Bose–Einstein condensates. The instability occurs at low pumping and in the absence of defects even in numerical simulations, and is justified rigorously on a theoretical basis by rewriting the laser master equation in the form of the complex Ginzburg–Landau equation (CGLE).^[91] This mathematical treatment can only be done for unidirectional lasers (Figure 5f) with fast gain dynamics and with a non-zero LEF, such as QCLs (Figure 1e). The only two parameters involved in the CGLE are mainly determined by the GVD and LEF of the laser. In the parameter space, it is possible to define different regions, delimited by the Benjamin–Feir lines, where a multimode instability may or may not occur. In ref., [26] it was shown that the QCL rings exhibiting a multimode regime belong to the instability region, close to the Benjamin–Feir lines.

Since these early studies, similarities with passive Kerr microcombs, such as multistability and the sech^2 spectral envelope, were highlighted. These insights have been consolidated in recent theoretical works that generalize the LLE by introducing a new single equation simultaneously capturing the physics of two distinct classes of frequency comb generators based on nonlinear active and passive optical media.^[16,70] Their formal unification makes it possible to establish a rigorous connection between the similar types of frequency comb spectra that can be observed in these systems. In addition, the generalized LLE also allows to study a hybrid device that combines several features of active and passive systems: it is a ring QCL driven by an external optical signal like a passive Kerr microresonator. In this way, the QCL is effectively transformed into a nonlinear driven-damped oscillator with interesting consequences: temporal solitons can form in the system (Figure 5g), in contrast to the FM character of free-running Fabry–Perot QCLs. In addition, a train of temporal solitons can be excited ad hoc in the cavity by means of appropriate write pulses, allowing one to manipulate the OFC in the spectral domain and create reconfigurable bit sequences that encode information within the cavity in the time domain.^[16] More generally, the spatiotemporal structures observed in the injected QCL system, such as Turing rolls and temporal solitons, are great examples of self-organizing phenomena in spatially extended dissipative systems studied in different branches of nonlinear physics. Moreover, a recent experimental demonstration has shown that such waveforms can also form spontaneously in the cavity without an external driving field, provided that the GVD is properly engineered.^[62] In this realization, the soliton pumping field is generated by direct electrical driving and arises at the zero crossing of the dispersion, resembling Cherenkov radiation. However, these dissipative Kerr solitons coexist with a dispersive wave and require spectral filtering outside the laser to be separated from the background (Figure 5h).

5. Perspectives

The QCL is like a phoenix that cyclically regenerates from its ashes: when in 2007 it seemed that most of the potential of this laser was already realized, the demonstration of coherent instabilities, and later of OFCs, opened new horizons. What makes the QCL so special among semiconductor lasers is its fast gain recovery: as reported here, this rapid carrier dynamics allows for a wide variety of frequency comb states, ranging from FM waveforms to temporal solitons. Now with the rapid advancement of

dual-comb spectroscopy, ring QCLs, and harmonic states, we are again at the beginning of an exciting phase of research in QCLs. QCL comb spectrometers could replace FTIRs in the near future, enabling millisecond time resolution with a large spectral bandwidth, opening up new opportunities in trace gas detection and real-time process analysis. The possibility of generating, extracting, and modulating sub-THz carriers in laser radio devices could offer an original approach in the development of ultrafast wireless communication systems. Our vision is that ring QCLs, thanks to their fast gain medium and the ability to engineer harmonic comb states, combine both a laser frequency comb source and a fast detector in one cavity, and thus do not require any heterogeneous integration for sub-THz photomixing. Finally, the increasing similarity in terms of behavior between these lasers and passive Kerr microresonators holds promise to make QCLs their active counterpart, extending the applications of solitons to the mid-infrared range for future battery-driven, miniaturized, turnkey spectrometers covering the molecular fingerprinting region. Further improvements in this direction should focus on the design of efficient light outcouplers, while paying attention not to perturb the physics of the ring multimode instability, as well as on the extension of the comb bandwidth.

Acknowledgements

Open Access Funding provided by Istituto Italiano di Tecnologia within the CRUI-CARE Agreement.

Conflict of Interest

The authors declare no conflict of interest.

Keywords

frequency-modulated combs, harmonic state, quantum cascade lasers, semiconductor laser frequency combs, semiconductor ring lasers, solitons

Received: July 23, 2021

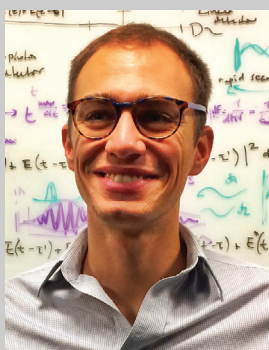
Revised: November 9, 2021

Published online:

- [1] C. L. Tang, H. Statz, G. Demars, *J. Appl. Phys.* **1963**, 34, 2289.
- [2] Y. I. Khanin, *Principles of Laser Dynamics*, North Holland, The Netherlands **1995**.
- [3] T. W. Hänsch, *Rev. Mod. Phys.* **2006**, 78, 1297.
- [4] T. Udem, R. Holzwarth, T. W. Hänsch, *Nature* **2002**, 416, 233.
- [5] S. T. Cundiff, J. Ye, *Rev. Mod. Phys.* **2003**, 75, 325.
- [6] N. Picqué, T. W. Hänsch, *Nat. Photon.* **2019**, 13, 146.
- [7] F. T. Arecchi, R. G. Harrison, *Instabilities and Chaos in Quantum Optics*, Vol. 34, Springer Science & Business Media, New York **2012**.
- [8] W. E. Lamb, *Phys. Rev.* **1964**, 134, 1429.
- [9] M. O. Scully, M. S. Zubairy, *Quantum Optics*, Cambridge University Press, Cambridge **1997**.
- [10] J. Faist, F. Capasso, D. L. Sivco, C. Sirtori, A. L. Hutchinson, A. Y. Cho, *Science* **1994**, 264, 553.
- [11] J. Faist, G. Villares, G. Scalari, M. Rosch, C. Bonzon, A. Hugi, M. Beck, *Nanophotonics* **2016**, 5, 272.

- [12] J. Faist, *Quantum Cascade Lasers*, Oxford University Press, Oxford 2013.
- [13] T. S. Mansuripur, C. Vernet, P. Chevalier, G. Aoust, B. Schwarz, F. Xie, C. Caneau, K. Lascola, C.-E. Zah, D. P. Caffey, T. Day, L. J. Missaggia, M. K. Connors, C. A. Wang, A. Belyanin, F. Capasso, *Phys. Rev. A* **2016**, 94, 063807.
- [14] H. Choi, L. Diehl, Z.-K. Wu, M. Giovannini, J. Faist, F. Capasso, T. B. Norris, *Phys. Rev. Lett.* **2008**, 100, 167401.
- [15] D. R. Bacon, J. R. Freeman, R. A. Mohandas, L. Li, E. Linfield, A. Davies, P. Dean, *Appl. Phys. Lett.* **2016**, 108, 081104.
- [16] L. Columbo, M. Piccardo, F. Prati, L. A. Lugiato, M. Brambilla, A. Gatti, C. Silvestri, M. Gioannini, N. Opačak, B. Schwarz, F. Capasso, *Phys. Rev. Lett.* **2021**, 126, 173903.
- [17] J. B. Khurgin, Y. Dikmelik, A. Hugi, J. Faist, *Appl. Phys. Lett.* **2014**, 104, 081118.
- [18] A. L. Schawlow, C. H. Townes, *Phys. Rev.* **1958**, 112, 1940.
- [19] C. Henry, *IEEE J. Quantum Electron.* **1982**, 18, 259.
- [20] M. F. Pereira, *Appl. Phys. Lett.* **2016**, 109, 222102.
- [21] N. Opačak, S. D. Cin, J. Hillbrand, B. Schwarz, *Phys. Rev. Lett.* **2021**, 127, 093902.
- [22] J. von Staden, T. Gensty, W. Elsässer, G. Giuliani, C. Mann, *Opt. Lett.* **2006**, 31, 2574.
- [23] M. S. Vitiello, L. Consolino, S. Bartalini, A. Taschin, A. Tredicucci, M. Inguscio, P. De Natale, *Nat. Photon.* **2012**, 6, 525.
- [24] L. Jumpertz, F. Michel, R. Pawlus, W. Elsässer, K. Schires, M. Carras, F. Grillot, *AIP Adv.* **2016**, 6, 015212.
- [25] N. Kumazaki, Y. Takagi, M. Ishihara, K. Kasahara, A. Sugiyama, N. Akikusa, T. Edamura, *Jpn J. Appl. Phys.* **2008**, 47, 6320.
- [26] M. Piccardo, B. Schwarz, D. Kazakov, M. Beiser, N. Opačak, Y. Wang, S. Jha, J. Hillbrand, M. Tamagnone, W. Chen, A. Zhu, L. Columbo, A. Belyanin, F. Capasso, *Nature* **2020**, 582, 360.
- [27] N. Opačak, F. Pilat, D. Kazakov, S. D. Cin, G. Ramer, B. Lendl, F. Capasso, B. Schwarz, *Optica* **2021**, 8, 1227.
- [28] N. Opačak, B. Schwarz, *Phys. Rev. Lett.* **2019**, 123, 243902.
- [29] A. Khalatpour, A. K. Paulsen, C. Deimert, Z. R. Wasilewski, Q. Hu, *Nat. Photon.* **2021**, 15, 16.
- [30] C. Y. Wang, L. Diehl, A. Gordon, C. Jirauschek, F. X. Kärtner, A. Belyanin, D. Bour, S. Corzine, G. Höfler, M. Troccoli, J. Faist, F. Capasso, *PRA* **2007**, 75, 031802.
- [31] A. Gordon, C. Y. Wang, L. Diehl, F. X. Kärtner, A. Belyanin, D. Bour, S. Corzine, G. Höfler, H. C. Liu, H. Schneider, T. Maier, M. Troccoli, J. Faist, F. Capasso, *Phys. Rev. A* **2008**, 77, 053804.
- [32] H. Risken, K. Nummedal, *J. Appl. Phys.* **1968**, 39, 4662.
- [33] R. Graham, H. Haken, *Zeitschrift für Physik* **1968**, 213, 420.
- [34] N. Yu, L. Diehl, E. Cubukcu, D. Bour, S. Corzine, G. Höfler, A. K. Wojcik, K. B. Crozier, A. Belyanin, F. Capasso, *Phys. Rev. Lett.* **2009**, 102, 013901.
- [35] A. K. Wójcik, N. Yu, L. Diehl, F. Capasso, A. Belyanin, *Phys. Rev. Lett.* **2011**, 106, 133902.
- [36] A. Hugi, G. Villares, S. Blaser, H. C. Liu, J. Faist, *Nature* **2012**, 492, 229.
- [37] D. Burghoff, T.-Y. Kao, N. Han, C. W. I. Chan, X. Cai, Y. Yang, D. J. Hayton, J.-R. Gao, J. L. Reno, Q. Hu, *Nat. Photon.* **2014**, 8, 462.
- [38] M. Rösch, G. Scalari, M. Beck, J. Faist, *Nat. Photon.* **2015**, 9, 42.
- [39] K. Garrasi, F. P. Mezzapesa, L. Salemi, L. Li, L. Consolino, S. Bartalini, P. De Natale, A. G. Davies, E. H. Linfield, M. S. Vitiello, *ACS Photon.* **2019**, 6, 73.
- [40] M. S. Vitiello, L. Consolino, M. Inguscio, P. D. Natale, *Nanophotonics* **2021**, 10, 187.
- [41] G. Villares, S. Riedi, J. Wolf, D. Kazakov, M. J. Süess, P. Jouy, M. Beck, J. Faist, *Optica* **2016**, 3, 252.
- [42] Y. Bidaux, F. Kapsalidis, P. Jouy, M. Beck, J. Faist, *Laser Photon. Rev.* **2018**, 12, 1700323.
- [43] F. P. Mezzapesa, L. Viti, L. Li, V. Pistore, S. Dhillon, A. G. Davies, E. H. Linfield, M. S. Vitiello, *Laser Photon. Rev.* **2021**, 15, 2000575.
- [44] F. Keilmann, C. Gohle, R. Holzwarth, *Opt. Lett.* **2004**, 29, 1542.
- [45] T. Ideguchi, A. Poisson, G. Guelachvili, N. Picqué, T. W. Hänsch, *Nat. Commun.* **2014**, 5, 3375.
- [46] I. Coddington, N. Newbury, W. Swann, *Optica* **2016**, 3, 414.
- [47] G. Villares, A. Hugi, S. Blaser, J. Faist, *Nat. Commun.* **2014**, 5, 5192.
- [48] H. Li, Z. Li, W. Wan, K. Zhou, X. Liao, S. Yang, C. Wang, J. C. Cao, H. Zeng, *ACS Photon.* **2020**, 7, 49.
- [49] L. Consolino, M. Nafa, M. De Regis, F. Cappelli, K. Garrasi, F. P. Mezzapesa, L. Li, A. G. Davies, E. H. Linfield, M. S. Vitiello, S. Bartalini, P. De Natale, *Communicat. Phys.* **2020**, 3, 69.
- [50] L. A. Sterczewski, J. Westberg, Y. Yang, D. Burghoff, J. Reno, Q. Hu, G. Wysocki, *ACS Photon.* **2020**, 7, 1082.
- [51] M. J. Norahan, R. Horvath, N. Woitzik, P. Jouy, F. Eigenmann, K. Gerwert, C. Kötting, *Anal. Chem.* **2021**, 93, 6779.
- [52] L. A. Sterczewski, J. Westberg, G. Wysocki, *Opt. Express* **2019**, 27, 23875.
- [53] L. Consolino, M. Nafa, F. Cappelli, K. Garrasi, F. P. Mezzapesa, L. Li, A. G. Davies, E. H. Linfield, M. S. Vitiello, P. De Natale, S. Bartalini, *Nat. Commun.* **2019**, 10, 2938.
- [54] H. Haus, *IEEE J. Quantum Electron.* **1975**, 11, 736.
- [55] M. Dong, S. T. Cundiff, H. G. Winful, *PRA* **2018**, 97, 053822.
- [56] M. Piccardo, P. Chevalier, B. Schwarz, D. Kazakov, Y. Wang, A. Belyanin, F. Capasso, *Phys. Rev. Lett.* **2019**, 122, 253901.
- [57] J. Hillbrand, D. Auth, M. Piccardo, N. Opačak, E. Gornik, G. Strasser, F. Capasso, S. Breuer, B. Schwarz, *Phys. Rev. Lett.* **2020**, 124, 023901.
- [58] I.-C. Benea-Chelmus, M. Rösch, G. Scalari, M. Beck, J. Faist, *PRA* **2017**, 96, 033821.
- [59] D. Burghoff, Y. Yang, D. J. Hayton, J.-R. Gao, J. L. Reno, Q. Hu, *Opt. Express* **2015**, 23, 1190.
- [60] M. Singleton, P. Jouy, M. Beck, J. Faist, *Optica* **2018**, 5, 948.
- [61] F. Cappelli, L. Consolino, G. Campo, I. Galli, D. Mazzotti, A. Campa, M. Siciliani de Cumis, P. Cancio Pastor, R. Eramo, M. Rösch, M. Beck, G. Scalari, J. Faist, P. De Natale, S. Bartalini, *Nat. Photon.* **2019**, 13, 562.
- [62] B. Meng, M. Singleton, J. Hillbrand, M. Franckić, M. Beck, J. Faist, *arXiv:2106.05078* **2021**.
- [63] N. Henry, D. Burghoff, Y. Yang, Q. Hu, J. B. Khurgin, *Opt. Eng.* **2017**, 57, 011009.
- [64] P. Tzenov, D. Burghoff, Q. Hu, C. Jirauschek, *Opt. Express* **2016**, 24, 23232.
- [65] D. Burghoff, *Optica* **2020**, 7, 1781.
- [66] T. S. Mansuripur, G. M. de Naurois, W. Metaferia, C. Junesand, S. Lourdudoss, B. Simozrag, M. Carras, F. Capasso, presented at, *Int. Quantum Cascade Lasers School and Workshop*, Policoro, Italy **2014**.
- [67] Q. Y. Lu, M. Raz ghi, S. Slivken, N. Bandyopadhyay, Y. Bai, W. J. Zhou, M. Chen, D. Heydari, A. Haddadi, R. McClintock, M. Amanti, C. Sirtori, *Appl. Phys. Lett.* **2015**, 106, 51105.
- [68] H. Li, P. Laffaille, D. Gacemi, M. Apfel, C. Sirtori, J. Leonard, G. Santarelli, M. Rösch, G. Scalari, M. Beck, J. Faist, W. Hänsel, R. Holzwarth, S. Barbieri, *Opt. Express* **2015**, 23, 33270.
- [69] R. L. Tober, J. D. Bruno, S. Suchalkin, G. Belenky, *J. Opt. Soc. Am. B* **2014**, 31, 2399.
- [70] F. Prati, M. Brambilla, M. Piccardo, L. Columbo, C. Silvestri, G. M. A. Gatti, L. Lugiato, F. Capasso, *Nanophotonics* **2020**, 10, 195.
- [71] D. Kazakov, M. Piccardo, P. Chevalier, T. S. Mansuripur, Y. Wang, F. Xie, C. en Zah, K. Lascola, A. Belyanin, F. Capasso, *Nat. Photon.* **2017**, 11, 789.
- [72] Y. Wang, A. Belyanin, *PRA* **2020**, 102, 013519.

- [73] M. Piccardo, P. Chevalier, T. S. Mansuripur, D. Kazakov, Y. Wang, N. A. Rubin, L. Meadowcroft, A. Belyanin, F. Capasso, *Opt. Express* **2018**, 26, 9464.
- [74] M. Piccardo, P. Chevalier, S. Anand, Y. Wang, D. Kazakov, E. A. Mejia, F. Xie, K. Lascola, A. Belyanin, F. Capasso, *Appl. Phys. Lett.* **2020**, 113, 031104.
- [75] M. Piccardo, P. Chevalier, B. Schwarz, Y. Wang, D. Kazakov, N. A. Rubin, S. Anand, E. A. Mejia, M. Tamagnone, F. Xie, K. Lascola, A. Belyanin, F. Capasso, in *Conf. on Lasers and Electro-Optics*, Optical Society of America, Washington, DC **2018**, FW3E.6.
- [76] M. Piccardo, D. Kazakov, N. A. Rubin, P. Chevalier, Y. Wang, F. Xie, K. Lascola, A. Belyanin, F. Capasso, *Optica* **2018**, 5, 475.
- [77] D. Kazakov, N. Opačak, M. Beiser, A. Belyanin, B. Schwarz, M. Piccardo, F. Capasso, *Optica* **2021**, 8, 1277.
- [78] Y.-C. Xin, Y. Li, V. Kovanis, A. L. Gray, L. Zhang, L. F. Lester, *Opt. Express* **2007**, 15, 7623.
- [79] Q. Lu, F. Wang, D. Wu, S. Slivken, M. Razeghi, *Nat. Commun.* **2019**, 10, 2403.
- [80] A. Forrer, Y. Wang, M. Beck, A. Belyanin, J. Faist, G. Scalari, *Appl. Phys. Lett.* **2021**, 118, 131112.
- [81] M. Piccardo, M. Tamagnone, B. Schwarz, P. Chevalier, N. A. Rubin, Y. Wang, C. A. Wang, M. K. Connors, D. McNulty, A. Belyanin, F. Capasso, *PNAS* **2019**, 116, 9181.
- [82] L. Consolino, A. Campa, M. De Regis, F. Cappelli, G. Scalari, J. Faist, M. Beck, M. Rösch, S. Bartalini, P. De Natale, *Laser Photon. Rev.* **2021**, 15, 2000417.
- [83] V. Pistore, H. Nong, P.-B. Vigneron, K. Garrasi, S. Houver, L. Li, A. Giles Davies, E. H. Linfield, J. Tignon, J. Mangeney, R. Colombelli, M. S. Vitiello, S. S. Dhillon, *Nat. Commun.* **2021**, 12, 1427.
- [84] J. Hillbrand, N. Opacak, M. Piccardo, H. Schneider, G. Strasser, F. Capasso, B. Schwarz, *Nat. Commun.* **2020**, 11, 5788.
- [85] C. Lin, Y. Xin, J. H. Kim, C. G. Christodoulou, L. F. Lester, *IEEE Photon. J.* **2009**, 1, 236.
- [86] T. Nagatsuma, G. Ducournau, C. C. Renaud, *Nat. Photon.* **2016**, 10, 371.
- [87] I. F. Akyildiz, J. M. Jornet, C. Han, *Phys. Commun.* **2014**, 12, (Supplement C), 16.
- [88] T. Kleine-Ostmann, T. Nagatsuma, *J. Infrared Millim. Terahertz Waves* **2011**, 32, 143.
- [89] E. Mujagić, S. Scharfner, L. K. Hoffmann, W. Schrenk, M. P. Semtsiv, M. Wienold, W. T. Masselink, G. Strasser, *Appl. Phys. Lett.* **2008**, 93, 011108.
- [90] B. Meng, M. Singleton, M. Shahmohammadi, F. Kapsalidis, R. Wang, M. Beck, J. Faist, *Optica* **2020**, 7, 162.
- [91] I. S. Aranson, L. Kramer, *Rev. Mod. Phys.* **2002**, 74, 99.
- [92] Z. Han, D. Ren, D. Burghoff, *Opt. Express* **2020**, 28, 6002.



Marco Piccardo is a researcher at the Istituto Italiano di Tecnologia in Milan leading a small team within the Vectorial Nano-Imaging research line. He is exploring novel approaches for structured light based on metasurfaces and in particular their integration in active laser cavities. He is also an associate researcher at Harvard University, where he did his postdoctoral studies exploring novel electronic and photonic properties of integrated laser frequency combs. He obtained his Ph.D. in physics in 2016 from Ecole Polytechnique working on the fundamental electronic processes responsible for the efficiency drop of blue light-emitting diodes at high-current operation, such as Anderson localization and Auger recombination. He received his B.Sc. in physics from Università degli Studi di Torino, and an M.Sc. in physics from Ecole Normale Supérieure and Ecole Polytechnique.



Federico Capasso is the Robert Wallace Professor of Applied Physics at Harvard University, which he joined in 2003 after 27 years at Bell Labs where he rose from postdoc to VP of Physical Research. He pioneered bandgap engineering of semiconductors, including the invention of the quantum cascade laser, and the field of flat optics with metasurfaces. He carried out high precision measurements of the Casimir force with MEMS and the first measurement of the repulsive Casimir-Lifshitz force. His awards include the Ives medal and Jarus Quinn prize of the Optical Society, the Fermi Prize of the Italian Physical Society, the Balzan prize for Applied Photonics, the King Faisal Prize for Science, the IEEE Edison Medal, the APS Arthur Schawlow Prize, the OSA Wood prize, the SPIE Gold Medal, the Rumford Prize of the American Academy of Arts and Sciences, the Franklin Institute Wetherill Medal, and the Materials Research Society Medal. He is a member of the National Academy of Sciences, the National Academy of Engineering, and the American Academy of Arts and Sciences.